

# A Nonparametric Bayesian Model for Synthesising Residential Solar Generation and Demand

Thomas Power, *Student Member, IEEE*, Gregor Verbič, *Senior Member, IEEE*,  
Archie C. Chapman, *Member, IEEE*,

**Abstract**—Increasing installations of distributed electricity generation have vastly increased the need for stochastic generation and demand data. However, the effects of such installations is uncertain, as high quality data is not always available before an installation is completed. In particular, there is a need for stochastic models of demand and generation profiles for unobserved *prosumers*. The model formulated in this paper bridges the gap between the limited available empirical data, and the large amount of high-quality, stochastic demand and generation data required for network and system analysis. The approach employs clustering analysis and a Dirichlet-categorical hierarchical model of the features of unobserved prosumers. Based on the data of clusters of prosumers, Markov chain models of demand and generation profiles are constructed from empirical data, and synthetic demand profiles are subsequently sampled from these. The sampled traces are cross-validated and show a good statistical fit to the observed data, and then two case studies are considered. The first identifies distinct behavioural differences in demand for residential areas of differing population density. The second case study varies levels of solar generation penetration, and shows that it contributes to significant intra-day demand variance, but has little impact on evening peak demand.

**Index Terms**—Prosumers, PV-battery systems, generic demand model, future grids.

## I. INTRODUCTION

MODERN power systems are increasingly characterised by changing patterns of “behind the meter” distributed energy resource (DER) use. In the coming decade, generation from rooftop PV is forecast to double, with solar projected to make up 8% of Australia’s total generation by 2030 [1]. Projections by the Australian Energy Market Operator (AEMO) [2] see energy generation capacity of rooftop photovoltaic systems rising from 4.3 GW in 2016 to 19 GW in 2035, thus becoming a major contributor to the flat forward trend in total power consumption that AEMO see out to 2035.

Rising penetrations of PV and battery storage technology present a number of challenges with regard to grid voltage. Chen et al. [3] investigate the impact of an increasing penetration of distributed generation on the voltage profiles of US distribution networks. They conclude that an increase in the penetration of distributed generation technologies results in an increasing incidence of voltage outside  $\pm 5\%$  of nominal connection voltage. This effect is similarly investigated by

Navarro-Espinosa and Ochoa in the UK [4], Widen, Wackelgard, Paatero and Lund in Sweden [5]. Further to this, Marzoughi, Verbič and Hill [6] investigate this impact with respect to the entire Australian National Electricity Market (NEM). In this study, they find that loadability in the network is generally higher where prosumers are inclined to follow proactive strategies with respect to power price. To manage this effect Tischer and Verbič [7] outline a system for managing residential power flows between electrical demand, PV systems, batteries and the grid. This involves a dynamic programming approach to optimise potential strategies. This is also explored by others [6], [8]–[13], who establish a basis for the implementation of price anticipating, or proactive SHERMS as being of benefit to the entire grid rather than price reactive SHERMS. Scott et al. [14] detail a methodology for optimising residential demand response strategies using stochastic inputs, which conducts online stochastic optimisation of PV and energy storage system control strategies. They conclude that stochastic optimisation is critical to achieving an optimal control strategy for residential power flows. This model illustrates that optimisation strategies such as these present a need for consistent, stochastic demand and generation data.

### A. Related work on Synthetic Demand and Generation Profiles

Much of the previous study on the synthesis of stochastic demand and generation profiles has centred around a ‘bottom-up’ approach. This particular framework is utilised by Widen, Nilsson and Wackelgard [15] to model building occupancy for the purposes of forecasting lighting demand. Their methodology involves simulating building occupancy as a Markov chain, defined by a state transition probability matrix. Richardson, Thompson and Infield [16] use a similar methodology for sampling building occupancy profiles, as do Page et al [17] among others [15]–[19]. McKenna and Thompson extend this methodology [16], [18], [19] in their high-resolution stochastic integrated thermal-electrical domestic demand model (the *CREST* model). Their particular occupancy model is central to the determination of a residence’s demand profile, and allows for a number of distinct day types, whereby it defines separate transition probability matrices for both weekdays and weekends, which captures weekly behavioural patterns. This is effective in that there are significant structural differences in the behaviour of household demand between weekends and weekdays. The generation component in the *CREST* model first involves sampling the weather conditions. Similarly to the demand model, a transition matrix is constructed from prior

Thomas Power, Gregor Verbič, and Archie C. Chapman are with the School of Electrical and Information Engineering, The University of Sydney, Sydney, New South Wales, Australia. e-mails: tpow5976, gregor.verbic, archie.chapman@sydney.edu.au.

historical data for the clearness index, which is a measure of the extent to which incident irradiance is blocked from reaching a PV module by cloud cover. In a method similar to that used by Hofmann et al. [20] and Bright et al [21], initial states are chosen at random, and the clearness index profile is sampled at each timestep through a repeated application of a state transition probability matrix [22]. This is then used to generate stochastic PV generation profiles [23], [24].

## B. Research Overview

This work develops a framework for producing a large collection of residential demand and generation profiles from limited observed data. Previous studies have either involved using a simplified probabilistic model [3], or reconstructing profiles using highly granular observed data, at great cost [22]. The methodology described in this paper requires data on a household level that is somewhat less granular, and more readily accessible. It also aims to retain the variance that is normally observed among observed demand and generation profiles. Part II of this paper details the formulation of the proposed model, while part III illustrates the following cross validation. Part IV outlines potential applications of the model through two specific case studies, while part V draws on these to outline the key conclusions of this work.

## II. MODEL FORMULATION

We wish to generate typical solar generation and demand profiles for a household according to specific features. These features can either be continuous or discrete, and may not be independently distributed within the data. Discrete features generally need no treatment prior to assignment. However, if the number of values taken on by numerical features is impractically large, some clustering analysis may be done, as described next. After this, the method used to identify a Markov chain model of the demand and solar generation profiles is described, followed by the steps used to generate new synthetic demand and generation traces.

### A. Feature-based Cluster Assignment

For this clustering analysis, only the continuous and larger discrete numerical features are included. The empirical data was collected during the *Ausgrid Smart-Grid Smart-City* (SGSC) project. Clustering is important because (i) considering each customer as a single category is computationally expensive, and (ii) it provides generalizable statistical information as the demand and PV generation in each set are correlated with their features.

Let  $n \in \mathcal{N}$  and  $m \in \mathcal{M}$  denote the set of observed and unobserved customers, respectively. Clustering analysis is run on empirical data to assign the  $n \in \mathcal{N}$  customers into representative sets, denoted  $k \in \mathcal{K}$  according to their features. The features of demand are the day types (weekday or weekend) and number of residents, while those for PV include the PV capacity, panel orientation and weather information. Clustering is completed using either  $k$ -means clustering [25] or *maximum a-posteriori Dirichlet process mixtures* (MAP-DP) clustering [26], which is useful for instances in which the number of clusters cannot be easily determined.

### B. Estimating the Dirichlet Distribution

After clustering, we could compute the frequencies,  $\{p_s\}_{k \in \mathcal{K}}$ , of each observed customer being a member a certain cluster. These values can be interpreted as the probability of a new, unobserved customer having certain features. However, they are only an estimate across the observed customers, and directly using them to allocate features fails to properly consider the error in this estimate, which can be significant where the fraction of customers observed is small. Thus, a Bayesian estimation approach is employed.

Specifically, the model uses the count of each  $k \in \mathcal{K}$  in the the observed  $\mathcal{N}$  as a hyperparameter of a Dirichlet distribution, which itself is sampled to yield a *categorical* probability distribution over the features for unobserved customers,  $m \in \mathcal{M}$ . Formally, this is given by:

$$\begin{aligned} \alpha & \quad \text{Vector of cluster counts} \\ \mathbf{q} \mid \alpha & \sim \text{Dir}(\alpha) \\ S_m \mid \mathbf{q} & \sim \text{Cat}(\mathbf{q}) \end{aligned}$$

In more detail, given the clusters, we use the Dirichlet distribution, given by the the probability density function:

$$f(\mathbf{q}_j; \alpha_j) = \frac{\Gamma(\alpha_{j0})}{\prod_{k=1}^m \Gamma(\alpha_{jk})} \prod_{k=1}^m q_{kj}^{\alpha_{jk}-1} \quad (1)$$

to overcome a limitation of previous models. Specifically, it accounts for variance in the distribution of features across unobservable customers, which is given in this case by:

$$\text{Cov}(Q_a, Q_b) = \begin{cases} \frac{-\alpha_a \alpha_b}{\alpha_0^2(\alpha_0+1)}, & \forall a \neq b \\ \frac{\alpha_a(\alpha_0 - \alpha_a)}{\alpha_0^2(\alpha_0+1)}, & \forall a = b \end{cases} \quad (2)$$

In this case,  $\mathbf{q}_j$  is the resultant probability measure for feature  $j$  drawn from the Dirichlet distribution, with individual elements  $q_{jk}$ , where  $k \in \{1, 2, \dots, m\}$ , and  $\sum_{k=1}^m q_k = 1$ , while the corresponding random probability measures and elements are given by  $\mathbf{Q}_j$  and  $Q_{jk}$ . The distribution is parametrised by  $\alpha_j$  which is given by:

$$\alpha_{jk} = \sum_{i=1}^n \delta_{c_{ij}, k}, \quad \forall j \leq u, \quad \forall k \leq m, \quad (3)$$

where  $\alpha_{j0} = \sum_{k=1}^m \alpha_{jk}$ , and  $\delta$  is the Kronecker delta. For each feature,  $\mathbf{q}_j$  parametrises a draw from a categorical distribution, such that for  $n^*$ , unobserved prosumers, we have:

$$\mathbf{A}_j^* = [A_{j1}^*, A_{j2}^*, \dots, A_{jm}^*], \quad (4)$$

which is defined by the probability density function:

$$f(\mathbf{A}_j^*; \mathbf{q}_j) = \frac{\Gamma(\sum_{k=1}^m A_{jk} + 1)}{\prod_{k=1}^m \Gamma(A_{jk} + 1)} \prod_{k=1}^m \mathbf{p}_k^{A_{jk}}. \quad (5)$$

This collection of feature counts defined by  $\mathbf{A}_j$  are then assigned to the unobserved prosumers.

### C. Demand Model

The demand model generates stochastic demand profiles for unobserved prosumers using observed data for characteristically similar prosumers. To do this, Markov chain modelling is used, with a state transition matrix defined for each timestep throughout the day. This model is time inhomogeneous, as there are structural differences in the behaviour of household energy usage at different points in the day. Once the timestep length and the collection of relevant observable customers have been defined, the state transition matrices are then constructed. For this study, a timestep of 30 minutes is used and as such, 48 different state transition matrices will be required to sample a profile over a 24 hour period. In addition to this, it will need to be specified whether the resulting profile is to be generated for a weekend or a weekday, as they have significantly different behaviour. Following this, the state transition matrices can be defined:

$$\mathbf{M} = [\mathbf{M}_1, \mathbf{M}_2, \dots, \mathbf{M}_{48}] \quad (6)$$

In each matrix  $\mathbf{M}_k$ , the states are defined for

$$m_{i,j,k}, \quad i, j \in \{0, 1, \dots, n\}, \quad (7)$$

and are used to represent the amount of energy consumed for the duration of timestep  $k$ . In the case of the validation data used in this work [27], the data is logged in terms of the number of kWh consumed in each relevant 30 minute period. In order to construct the state transition probability matrices, these readings are discretised with each kWh reading rounded to the nearest 0.01 kWh, and the possible attainable states are defined as being this value multiplied by 100. The state, therefore, of a reading of 1.023 kWh will be 102. These states are defined up to an arbitrary maximum limit  $n$ , which is set well above the maximum observed state. The state transition probability matrices are built up from the observed data by taking:

$$m_{i,j,k} = \sum_{h=1}^N \delta_{x_{hk-1},i} \delta_{x_{hk},j}, \quad (8)$$

over each similar observed prosumer in the available data. Stochastic demand profiles can then be directly sampled from this set of matrices by first calculating the conditional distribution of the initial state, which is given by:

$$\mathbf{p} = [p_1, p_2, \dots, p_n], \quad p_j = \frac{\sum_{i=1}^n m_{i,j,1}}{\sum_{i=1}^n \sum_{j=1}^n m_{i,j,1}}. \quad (9)$$

Once this initial state  $s_1$  is drawn from the categorical distribution parametrised by  $\mathbf{p}$ , subsequent states for the remainder of the day can be drawn from the following matrices. For each state  $s_k$ , the associated probability measure is derived from  $\mathbf{M}_{s_{k-1},j,k}$  using kernel density estimation [28]. Gaussian kernel density estimation is used to make each state attainable, even if it has not been observed in the data. It is given by:

$$p_{s_{k-1},j,k} = \frac{\sum_{j^*=1}^n m_{s_{k-1},j^*,k} \exp\left(-\frac{(j-j^*)^2}{2h^2}\right)}{\sum_{j^*=1}^n \exp\left(-\frac{(j-j^*)^2}{2h^2}\right)} \quad (10)$$

From this kernel density estimate, the state  $s_k$  can be drawn from a categorical distribution:

$$s_k \sim \text{Cat}(\mathbf{p}_{s_{k-1},k}) \quad (11)$$

Before generating these profiles, it will need to be specified whether the the profiles are to be generated for a weekday or a weekend. There are significant structural differences in energy usage behaviour between weekdays and weekends [29], and as such, only observed data from weekdays is to be used to generate weekday profiles, while only observed data from weekends is to be used to calculate weekend profiles.

One important property of the Dirichlet process is its clustering property [30]–[32]. This allows for the generation of samples that have a tendency to follow recurring trajectories and sequences of states [33]. This sampling process involves reinforcement, where the state sampled is added into the initial matrix of counts. In this way, states and sequences of states that have previously been sampled more often have a higher chance of being sampled again, and recurring behaviours will start to arise. With a slight variation to the method mentioned previously, this is sampled directly using the Dirichlet distribution, and is analogous to a draw from an infinite Polya Urn process [34], [35]. First, the set of state transition matrices  $\mathbf{M}$  is taken, and Gaussian kernel smoothing [36] is applied to each row, such that each row defines a probability measure, denoted by  $\mathbf{M}^*$ . In contrast to the previous method, each row of  $\mathbf{M}^*$  is used as a prior set of counts for a Dirichlet distribution.

Second, a set of state transition matrices is drawn from the Dirichlet distribution specifically for each unobserved prosumer, thereby giving each prosumer unique sets of transition probabilities, analogous to energy consumption behaviours. These state transition matrices are therefore denoted by  $\mathbf{P}^*$ , where

$$[P_{i,1,k}^*, P_{i,2,k}^*, \dots, P_{i,n,k}^*] \sim \text{Dir}([m_{i,1,k}^*, m_{i,2,k}^*, \dots, m_{i,n,k}^*]), \quad (12)$$

where  $\text{Dir}(\alpha)$  denotes a draw from the Dirichlet distribution parameterised by  $\alpha$ .

Third, sampling from this set of state transition matrices is done similarly to the general method outlined previously. To appropriately simulate differing behaviour between prosumers, a new set of state transition matrices will have to be drawn from (13) for each prosumer.

### D. Generation Model

The generation model is the third key component in this model. It is intended to synthesise solar generation data in order to compile stochastic daily profiles similar to the demand model mentioned previously. This generation model was developed and described in detail in a previous work [37], and utilises a Markov chain framework similar to that provided by the CREST model [16], [18], [19]. In this model, solar PV generation is modelled using the following formula:

$$P = \eta A(TIF)(CI)G, \quad (13)$$

where  $\eta$  is the efficiency of the PV module, and  $A$  is the area of the module. For the purposes of this work,  $TIF$  is

the ‘time irradiance factor’, and is a measure of the incident irradiance on a PV module with respect to the latitude of the panel, orientation, time of day and time of year.  $G$  is the extraterrestrial irradiance constant, while  $CI$  is the clearness index, which represents the extent to which cloud cover obstructs irradiance of the panel. This is the stochastic quantity that this model emulates. As detailed in previous work [37], the clearness index for a particular prosumer is sampled from a single state transition probability matrix, which is constructed from observed generation data. This is substituted into (20) to obtain stochastic PV generation values for each timestep of the day.

### III. MODEL VALIDATION

#### A. Feature Assignment

The following section details the results of a cross validation of the model using data sourced from Ausgrid’s ‘Smart Grid, Smart City’ (SGSC) data set [38]. This data contains a three year sample of half hourly household demand and generation measurements for approximately 13,000 households. Following model cross validation, a number of case studies are then conducted to demonstrate potential applications. The first of these makes use of the variation in geography evident in the SGSC data set. The model is used to investigate if there are structural behavioural differences between demand and generation profiles in dense urban, suburban, and rural settings and compares and contrasts these. The second case study investigates the effect on aggregated generation and net demand profiles of an increasing penetration of distributed generation systems.

#### B. Cross Validation

The first part of this framework involves the clustering and assignment module. For the SGSC data set, the peak readings for solar installations are the only relevant variable available for clustering, as they act as a proxy for the capacity of the system. The distribution of the 189 observations of this variable is shown in Fig. 1, and it is this data which is used as the input for both  $k$ -means and MAP-DP clustering. One of the limitations of  $k$ -means clustering is that the number of clusters and prior estimates for cluster location are required before running the algorithm. These are therefore chosen using the peaks of the histogram in Fig. 1, and the results are detailed in Table I for a varying number of clusters.

It is fairly evident from this table that the selection of prior cluster locations is fairly arbitrary, and in this case, prior cluster centroids have been chosen to coincide with the peaks of the histogram in Fig. 1. The squared error of the cluster assignment is used as an appropriate metric to determine the effectiveness of the assignment, given in Table I as ‘Error’. This metric is the sum of the squared distance of each point from its respective cluster centroid, given by:

$$Error = \sum_{u_i \in U} \sum_{x_i | z_i = u_i} (x_i - u_i)^2, \quad (14)$$

where  $U = \{u_1, u_2, \dots, u_k\}$  is the set of cluster centroids,  $\mathbf{x} = \{x_1, x_2, \dots, x_n\}$  is the original set of data points, and

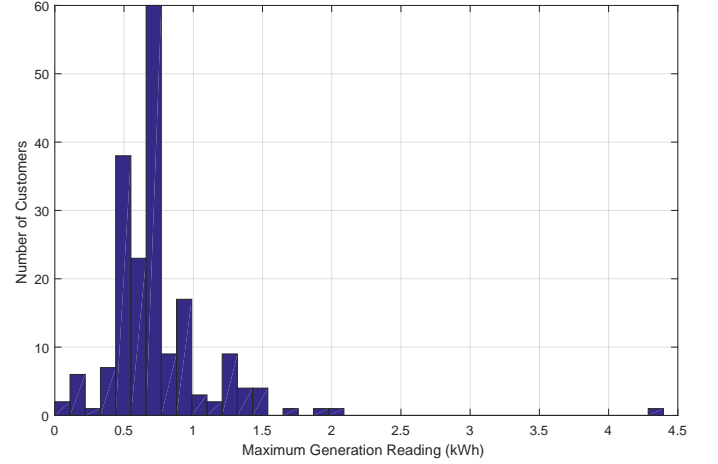


Fig. 1. Histogram of peak solar readings for all observed generators.

TABLE I  
RESULTS OF  $k$ -MEANS CLUSTERING ANALYSIS ON PEAK SOLAR READINGS

Cluster	1	2	3	4	5	6	7	8	Error
Estimate	0.75	-	-	-	-	-	-	-	-
Calculated	0.74	-	-	-	-	-	-	-	-
Population	189	-	-	-	-	-	-	-	15.98
Estimate	0.5	0.75	-	-	-	-	-	-	-
Calculated	0.62	1.49	-	-	-	-	-	-	-
Population	164	25	-	-	-	-	-	-	7.74
Estimate	0.5	0.75	1.5	-	-	-	-	-	-
Calculated	0.42	0.73	1.53	-	-	-	-	-	-
Population	55	111	23	-	-	-	-	-	5.93
Estimate	0.5	0.75	1.5	2.0	-	-	-	-	-
Calculated	0.42	0.73	1.37	4.39	-	-	-	-	-
Population	55	109	24	1	-	-	-	-	1.61
Estimate	0.25	0.5	0.75	1.5	2.0	-	-	-	-
Calculated	0.17	0.47	0.73	1.37	4.39	-	-	-	-
Population	9	48	107	24	1	-	-	-	1.27
Estimate	0.25	0.5	0.75	1.5	2.0	4.5	-	-	-
Calculated	0.17	0.47	0.73	1.29	1.88	4.39	-	-	-
Population	9	48	106	22	3	1	-	-	0.88
Estimate	0.25	0.5	0.75	1.0	1.5	2.0	4.5	-	-
Calculated	0.17	0.47	0.67	0.92	1.32	1.88	4.39	-	-
Population	9	46	83	28	19	3	1	-	0.29
Estimate	0.25	0.5	0.75	1.0	1.25	1.5	2.0	4.5	-
Calculated	0.17	0.47	0.67	0.91	1.25	1.45	1.88	4.39	-
Population	9	46	83	27	14	6	3	1	0.22

$\mathbf{z} = \{z_1, z_2, \dots, z_n\}$  are the respective cluster assignments of these data points. This is also the metric that is minimised by the  $k$ -means algorithm [36]. It is evident from Table I, that the marginal improvement in the error diminishes with each additional cluster, and therefore there is a smaller improvement in accuracy with the increase in complexity of the model.

The MAP-DP clustering algorithm detailed by Raykov et al. [26], is an alternative to the  $k$ -means algorithm detailed previously. For this algorithm, an initial cluster mean and variance is specified, along with a prior estimate for the variance of new clusters and the Dirichlet parameter  $\alpha$ , which represents the propensity of the algorithm to pick new clusters for assignments. In the case of the peak solar reading data, this clustering algorithm was run with the naive prior cluster mean being the mean of the data:

$$\frac{1}{n} \sum_{i=1}^n x_i = 0.7428, \quad (15)$$

and the prior cluster variance was given as the data variance:

$$\frac{1}{n-1} \sum_{i=1}^n (x_i - \bar{x})^2 = 0.1700, \quad (16)$$

Using these values, the MAP-DP algorithm was run using a Dirichlet parameter of 9, which yielded the following 4 clusters shown in Table II:

TABLE II  
RESULTS OF MAP-DP CLUSTERING WITH A DIRICHLET PARAMETER OF 9

Cluster ( $i$ )	1	2	3	4
Location ( $\bar{x}_i$ )	0.6368	1.3293	1.8843	4.3960
Variance ( $s_i$ )	0.0338	0.0104	0.016	0
Population ( $n_i$ )	165	20	3	1

A superposition of these clusters comprise a Gaussian mixture model, which is then normalised for assignments to unobserved prosumers, this is given by the following probability mass function:

$$f(x) = \frac{\sum_{i=1}^N \frac{1}{\sqrt{2\pi s_i^2}} e^{-\frac{(x-\bar{x}_i)^2}{2s_i^2}}}{\sum_{i=1}^N n_i}, \quad (17)$$

where  $\bar{x}_i$  is the mean,  $s_i$  is the variance and  $n_i$  is the population of cluster  $i$ . The MAP-DP clustering analysis has therefore revealed a set of three Gaussian distributed clusters from which this peak solar data is distributed. In contrast to the  $k$ -means algorithm, this analysis did not require prior knowledge of cluster centroids or variances, but only an estimate for the Dirichlet parameter. This makes the MAP-DP algorithm much more versatile where little is known about the subject data. Once these features are clustered, the resulting set of clusters can be used to parametrise a Dirichlet distribution. This defines a distribution for the probability measure for the assignments, thereby giving it a variance as well as an expected value.

TABLE III  
A SEQUENCE OF DRAWS FROM A DIRICHLET DISTRIBUTION  
PARAMETRISED BY  $k$ -MEANS CLUSTERED PEAK SOLAR OUTPUT DATA

Draw	$q_1$	$q_2$	$q_3$	$q_4$	$q_5$	$q_6$
1	0.0116	0.2472	0.5847	0.1385	0.0091	0.0089
2	0.0398	0.2955	0.5215	0.1305	0.0069	0.0056
3	0.0666	0.2744	0.5478	0.0924	0.0118	0.0068
4	0.0519	0.2124	0.5776	0.1338	0.0213	0.0029
5	0.0570	0.2065	0.5767	0.1353	0.0237	0.0008
6	0.0435	0.2439	0.6081	0.0901	0.0122	0.0022
7	0.0707	0.2723	0.5579	0.0964	0.0026	0.0001
8	0.0541	0.2813	0.5049	0.1344	0.0210	0.0043
9	0.0413	0.2610	0.5757	0.1133	0.0078	0.0008
10	0.0188	0.2987	0.5325	0.1310	0.0089	0.0102
Observed	0.0476	0.2540	0.5608	0.1164	0.0159	0.0053
Mean	0.0476	0.2540	0.5608	0.1164	0.0159	0.0053
Variance	0.0002	0.0010	0.0013	0.0005	0.0001	0.0001

Following the sampling from a Dirichlet distribution, the counts of each feature can then be drawn from a categorical distribution parametrised by this sample. For the samples in Table 6.4, the feature counts are given in Table IV based on an assignment to 100 unobservable prosumers. These counts are given by  $\mathbf{c} = [c_1, c_2, \dots, c_6]$ .

TABLE IV  
A SEQUENCE OF DRAWS FROM A CATEGORICAL DISTRIBUTION  
PARAMETRISED BY THE PROBABILITY MEASURES IN TABLE III

Draw	$c_1$	$c_2$	$c_3$	$c_4$	$c_5$	$c_6$
1	0	26	57	17	0	0
2	2	35	51	11	0	1
3	4	30	54	11	1	0
4	4	25	58	8	4	1
5	4	19	68	9	0	0
6	1	25	68	4	2	0
7	9	24	57	10	0	0
8	6	35	47	9	2	1
9	2	38	55	5	0	0
10	0	28	59	11	2	0

It is therefore evident that the model can successfully emulate the variance in the estimation of the distribution of features, as shown in table III

### C. Demand Model Validation

The function of the demand module in this model is to take a collection of demand data from observed prosumers as an input, and to generate either daily or multiple day profiles based on this data. Following the assignment of features to unobserved prosumers, the set  $\mathbf{M}$ , of state transition matrices can then be populated using observed data from prosumers sharing similar features. In this case, the set of matrices is limited to  $700 \times 700 \times 48$ , which corresponds to the maximum demand being 7 kWh over a half-hour period. In order to conduct a cross-validation of this model, the generated profiles are compared to those observed from a separate subset of the data to check for similarity. In order for this cross validation to be valid, subsets of the data need to be taken such that they do not contain any nested statistical factors. As such, the data random selection of 1000 prosumers are used for the model construction, and a separate random subset of another 1000 prosumers is used for cross validation. The matrices calculated using this process are large and sparse, and as such, and as such, the state transition matrix at 6:00pm on weekdays is visualised for states 0 to 100 as a heatmap in 2.

As these matrices are sparse, the following logarithmic transform of the counts is used for  $m_{ijk} \in M_i$ :

$$m_{ijk}^* = \log_{10}|m_{ijk}| \quad i, j \in \{1, 2, \dots, 100\} \quad (18)$$

The heatmap shown in figure 2, uses red to denote a high count, while blue indicates a low count. Each pixel represents a distinct state transition count, with the previous state, or state before 6:00pm denoted by the row, and the state after 6:00pm denoted by the column.

It can therefore be seen from Fig. 2, that a majority of transitions take place from states near zero, to similar states near zero. There are two major features to this data, the first of which is that transitions to higher states tend to be less likely than transitions to lower states. The second feature of this visualisation is that transitions to similar states are more likely than transitions to dissimilar states. From this set of matrices, profiles can be sampled directly, as shown in 3.

When aggregated, however, it is apparent that the mean of this synthetic data matches that of the observed data. This

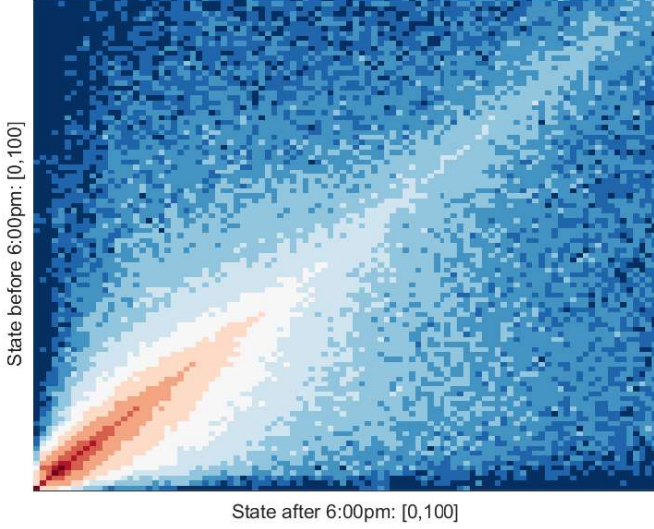


Fig. 2. Logarithmic heatmap of the Markov state transition matrix calculated at 6:00pm for 1000 prosumers

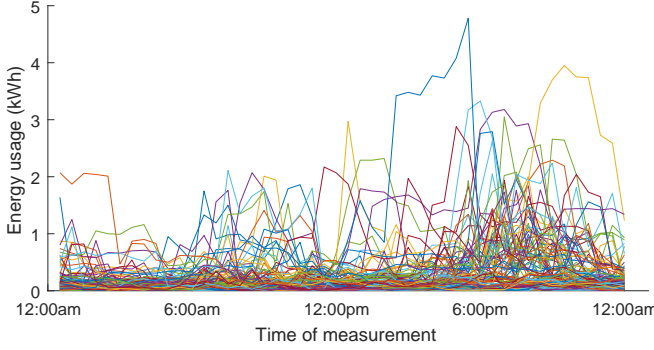


Fig. 3. 100 synthetic weekday demand profiles generated from 1000 prosumers

is illustrated in Fig. 3. This figure shows the aggregate of 1000 synthetic profiles in comparison to the aggregate of 1000 observed profiles populated from separate data. It is visually clear that the data generated by the model shows similar behaviour to the observed data. In order to better quantify this, the mean absolute error of the estimate given by the synthesised profiles is calculated. This is given by:

$$\text{Mean Absolute Error} = \frac{1}{48} \sum_{i=1}^{48} \frac{|x_i - x_i^*|}{x_i}, \quad (19)$$

where 48 is the number of samples in the daily profile,  $x_i$  is the observed value at timestep  $i$ , and  $x_i^*$  is the synthesized value at timestep  $i$ . The mean absolute error is calculated for the weekday profile to be 9.80%. Given that the samples range between approximately 200 kWh and 500 kWh over the course of a day, this error rate is small compared to the range of the observed data itself. It is therefore evident that the model can accurately represent the behaviour of observed data. It is also evident that a large amount of information is lost when modelling is done using the aggregate, as the information on the variability of individual profiles is not retained.

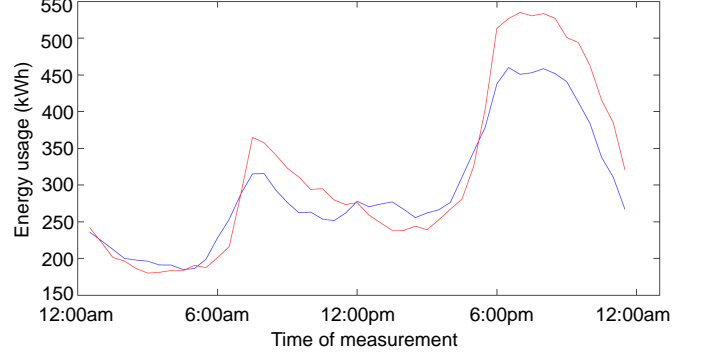


Fig. 4. 1000 aggregated observed weekday demand profiles (red) and 1000 synthesized profiles (blue)

#### D. Multiple Day Profiles

Using the methodology outlined in section II, the demand model can be extended to produce multiple day profiles for each specific unobserved customer. Fig. 5 illustrates an observed 20 day profile from the SGSC dataset.

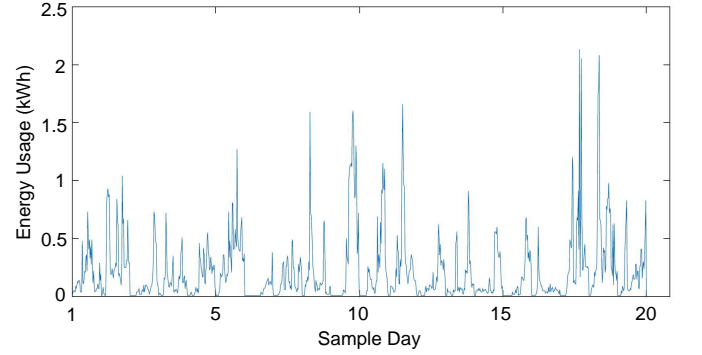


Fig. 5. 20 day demand profile generated from 1000 observed prosumers

Similarly to Fig. 5, 6 illustrates an example of an observed 20 day demand profile.

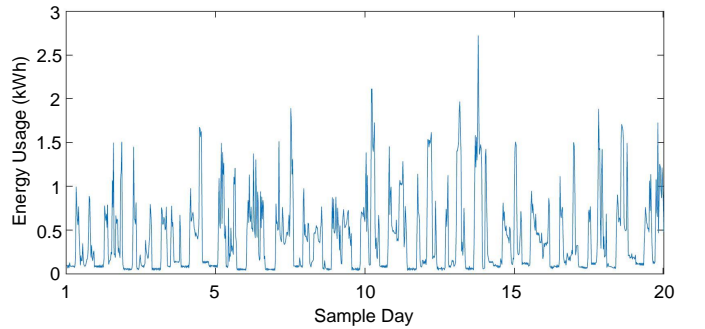


Fig. 6. 20 day demand profile sampled from observed data

Some degree of habitual daily behaviour is evident in each of these profiles. To quantify this effect, the autocorrelation is calculated for each sample with a 48 timestep lag. This mea-



sures the correlation between each day and the day preceding it, which is given by [39] as:

$$R(\mathbf{x}, n) = \frac{1}{(N - n)s^2} \sum_{t=1}^{N-n} (x_t - \bar{x})(x_{t+n} - \bar{x}) \quad (20)$$

Where  $n$  is the lag in timesteps,  $s^2$  is the sample variance, and  $N$  is the total number of samples. The autocorrelation in this case calculates the correlation between any sample  $x_{t+n}$  and the corresponding sample  $x_t$  at  $n$  steps beforehand. Using  $n = 48$  allows for the correlation between daily behaviours to be quantified. In this particular case, the observed profile had a calculated daily autocorrelation of 0.3066, while the generated profile was 0.1993. This shows that in this case, the generated profile does emulate habitual daily behaviour to a large extent, but does not entirely reproduce the habitual behaviour in the observed sample. This is also evident in an average autocorrelation taken over ten synthetic samples and ten observed samples, which yielded 0.1429 and 0.3584 respectively.

#### E. Generation Model Validation

Similarly to the demand model, the generation model is cross-validated using the SGSC data set. Using the methodology outlined in previous work [37], a clearness index state transition matrix is generated using data from 90 prosumers over the 3 year sample period. This is illustrated in , in which a number of key features are evident. Firstly, it is apparent that

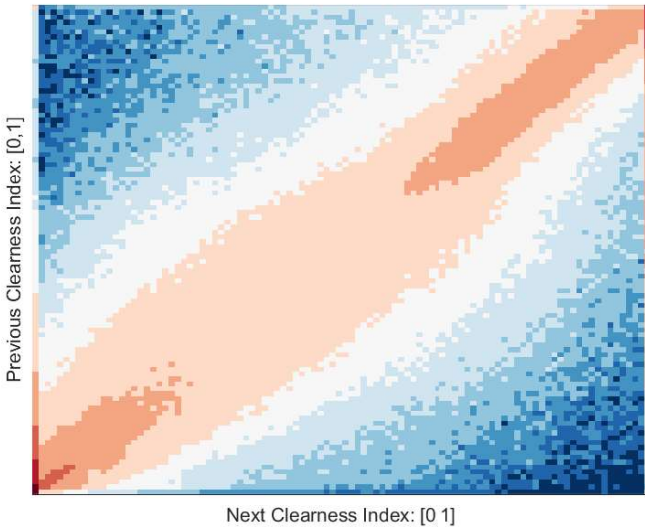


Fig. 7. Clearness index state transition probability heatmap for 90 observed prosumers

the distribution of clearness index state transitions is bi-modal, with transitions being more likely from low indices to low indices, and high indices to high indices, shown in red. There is also a discontinuity at clearness indices 0 and 1 exactly, at the extreme left and right columns of the figure respectively. Transitions to these states are relatively likely, and transitions from these states are relatively unlikely. This shows that the clearness index has a tendency to transition towards 0 and 1.

Following the population of the clearness index state transition matrix, profiles can be generated. In Fig. , the aggregate of 100 synthesized profiles is shown in red, generated for the approximate location of Sydney city in March. These profiles have been generated similarly to those detailed in [37]. These are shown along with 100 aggregated observed profiles, which are shown in red. From Fig. 8, it is clear that the synthetic

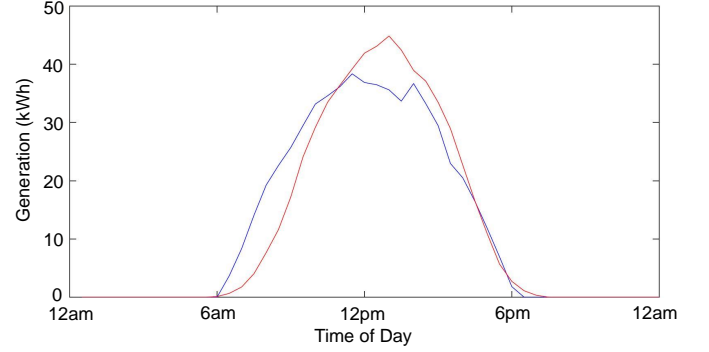


Fig. 8. 100 aggregated synthetic solar profiles (blue), and 100 aggregated observed solar profiles (red)

solar profiles follow a similar curve to the observed profiles over the course of the day. Given that only 100 profiles were used in this case, the variance is higher than in the demand model cross validation mentioned previously. The maximum absolute error in the estimate occurs at 8:00am, and is 11.6 kWh. Maximum absolute error is used in this case as the mean absolute error metric defined for the generation module cross validation is not effective in this case. This is due to the fact that the values approach zero before approximately 6:00am and after approximately 6:00pm, and the percentage error in these cases does not effectively represent the accuracy of the estimation.

## IV. CASE STUDIES

### A. Case Study: Geographical Variation

In order to demonstrate some of the potential applications of this model, two specific case studies have been conducted. The first of these illustrates differences in demand behaviour between rural, urban and suburban postcodes on both weekdays and weekends. For this study, three postcodes were selected. These are the urban Sydney suburb of Surry Hills, with 276 observed prosumers, Suburban Newcastle, with 832 prosumers, and the rural town of Pokolbin, with 266 prosumers. Using data from these prosumers, demand state transition matrices were compiled for each postcode and 1000 synthetic profiles were generated for each. The aggregated results for weekday demand are detailed in Fig. 9. It is apparent from this figure that the 1000 simulated residences in Pokolbin, shown in green, have a generally higher demand than those in Newcastle, shown in red, and Surry Hills, shown in blue. It is evident that the morning peak in each profile occurs at approximately the same time, being 7:00am - 8:00am. There is a difference, however, in the afternoon peak, which occurs just after 6:00pm for Pokolbin, with Newcastle peaking just after,

and Surry Hills peaking later, at about 8:00pm. In addition to this, the Pokolbin profile appears to have a much bigger morning peak relative to the level of demand over the middle of the day, while the morning peak in Newcastle and Surry Hills is lower.

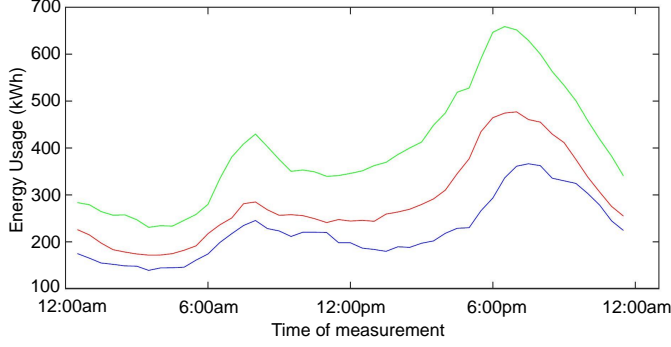


Fig. 9. 1000 aggregated weekday synthetic demand profiles for Surry Hills (Blue), Newcastle (Red) and Pokolbin (Green)

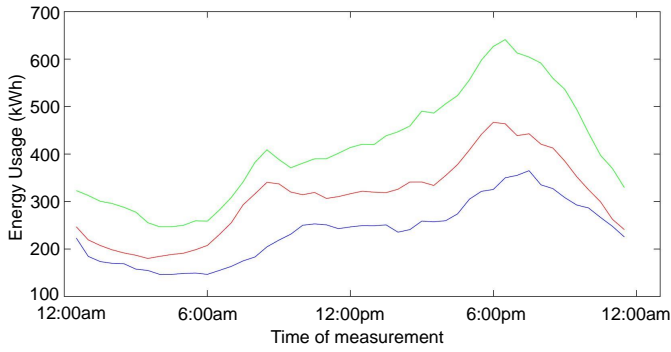


Fig. 10. 1000 aggregated weekend synthetic demand profiles for Surry Hills (Blue), Newcastle (Red) and Pokolbin (Green)

Fig. 10 details this same set of aggregated profiles generated from weekend data. One of the major differences is that for all three postcodes, is that demand during the middle of the day is higher. Both Newcastle and Pokolbin have a morning peak at a similar time to weekdays, however Surry Hills has a lowered morning peak, which occurs at around 10:00am-11:00am. For each of the three profiles, demand does not drop significantly after the morning peak, but instead stabilises, or rises throughout the day. In contrast to this, the evening peak and overnight profile does not differ significantly from the weekday profiles.

This case study demonstrates the application of this model to the generation of load profiles in specific areas. The model was therefore able to generate 1000 daily profiles for each postcode, using less than 300 prosumers to populate the Pokolbin and Surry Hills models, and approximately 830 prosumers to populate the Newcastle model. This method has applications to the analysis of aggregated loads at the ends of distribution feeders, or even certain zone substations, where only a limited amount of observed data are available.

### B. Case Study: Increasing Solar Penetration

The purpose of this case study is to demonstrate the function of the model to simulate the distribution of solar generation amongst a population, given a small set of observed data, and to investigate the effect on net demand profiles with increasing penetrations of installed solar generation. For this case study, the postcode 2280 is used, this corresponds to the southern suburbs in Newcastle. This postcode is an excellent candidate for this study as it has a large amount of observed demand data available in the SGSC dataset, and in addition, also has 61 prosumers with observed solar data available. This means that of the 225 observed customers with data available, 27.11% of these have installed solar generation. For this case study, a set of 1000 unobservable prosumers is used.

In the sampling of the aggregate solar load profile, the same clearness index transition profile was used for every prosumer, as they are tightly grouped geographically. This replicates the effect of the suburb experiencing the similar transitions in cloud cover. Following the formulation of an aggregate generation profile, this is subtracted from the demand profile to yield a net demand profile. This is given for 27.1% penetration in Fig. 11. In order to illustrate the variance of these net demand profiles, a collection of ten separate net demand profiles are plotted, along with the original gross demand profile plotted in red.

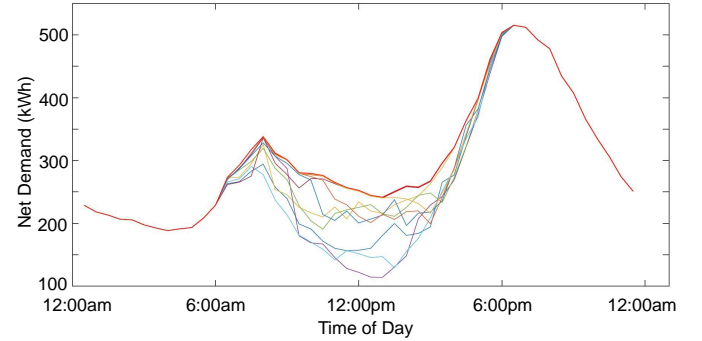


Fig. 11. 10 weekday net demand profiles, with gross demand profile (Red) for 1000 prosumers in the 2280 postcode, with 27.1% solar penetration.

There are a number of clear features in Fig. 11, the first of these is that the impact of the distributed generation is the greatest during the midday low. On particularly sunny days, there is a lessened morning peak, however the evening peak remains largely unchanged.

Fig. 12 outlines a similar plot of synthesized profiles for a distributed generation penetration of 80%.

Fig. 12 exhibits more pronounced behaviour than Fig. 11, with net demand becoming negative over the midday low on some days. One feature which remains common to these charts is that the evening peak is largely unchanged from its gross demand value. It is therefore evident that the level of distributed generation penetration has little impact on the daily peak residential demand, which is the evening peak. In this case study, the solar profiles are generated for early March, and as such it is expected that the evening peak will be similarly unaffected from March to September.



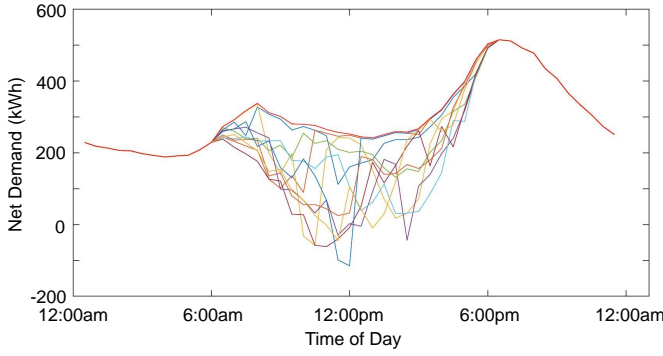


Fig. 12. 10 weekday net demand profiles, with gross demand profile (Red) for 1000 prosumers in the 2280 postcode, with 80% solar penetration.

In addition to these charts, Fig. 13 details the average net demand profile for 27%, 40%, 50%, 60%, 80% and 100% distributed generation penetration. It can be seen that the improvement on the current net demand profile, given by 27% penetration, is significant over the morning peak and midday low. The average improvement on the evening peak is very minimal.

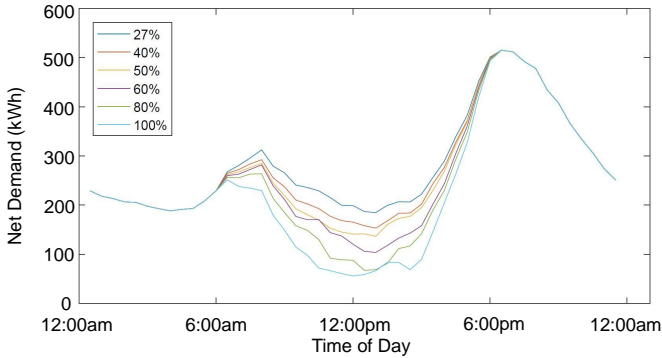


Fig. 13. Average weekday net demand profiles for 1000 prosumers in the 2280 postcode with various levels of solar penetration

This case study has therefore been able to demonstrate the effect of rising penetrations of distributed generation both on average, and in individual profiles. The clustering and assignment portions of the model were able to successfully assign generation features to unobservable prosumers, and stochastic demand and generation profiles could be generated. While 1000 prosumers were used for this case study, it could easily be extended in order to model a set of prosumers on a particular LV distribution network, or even the set of prosumers supplied from a particular zone substation.

## V. CONCLUSION

This paper demonstrates a tool for estimating and generating synthetic residential demand and generation data. It uses a Bayesian framework to probabilistically simulate unobserved prosumers, and thus exhibits a strength in modelling with sparse input data. It is envisioned that future work with this model will allow for the modelling and simulation of planned

residential solar and demand control schemes at low cost for input data acquisition.

## REFERENCES

- [1] Australian Government Department of the Environment and Energy, "Australia's Emissions Projections 2016," <https://www.environment.gov.au/system/files/resources/9437fe27-64f4-4d16-b3f1-4e03c2f7b0d7/files/aust-emissions-projections-2016.pdf>, [Accessed: June 5, 2017].
- [2] AEMO, "National Electricity Forecasting Report, 2016," <https://www.aemo.com.au/Electricity/National-Electricity-Market-NEM/Planning-and-forecasting/National-Electricity-Forecasting-Report>, [Accessed: June 5, 2017].
- [3] P. Chen, R. Salcedo, Q. Zhu, F. de Leon, D. Czarkowski, Z. Jiang, V. Spitsa, Z. Zabar, and R. Uosef, "Analysis of voltage profile problems due to the penetration of distributed generation in low voltage secondary distribution networks," *IEEE Transactions on Power Delivery*, vol. 27, no. 4, pp. 2020–2028, 2012.
- [4] A. Navarro-Espinosa and L. Ochoa, "Probabilistic impact assessment of low carbon technologies in lv distribution systems," *IEEE Transactions on Power Systems*, vol. 31, no. 3, pp. 2192–2203, 2016.
- [5] J. Widen, E. Wackelgard, J. Paatero, and P. Lind, "Impacts of distributed photovoltaics on network voltages: Stochastic simulations of three swedish low-voltage distribution grids," *Electric Power Systems Research*, vol. 80, no. 12, pp. 1562–1571, 2010.
- [6] H. Marzoughi, G. Verbič, and D. Hill, "Aggregated demand response modelling for future grid scenarios," *Sustainable Energy Grids and Networks*, vol. 5, pp. 94–104, 2016.
- [7] H. Tischer and G. Verbič, "Towards a smart home energy management system - a dynamic programming approach," *2011 IEEE PES Innovative Smart Grid Technologies*, no. 4, pp. 1–7, 2011.
- [8] C. Keerthisinghe, A. Chapman, and G. Verbič, "Energy management of pv-storage systems: Policy approximations using machine learning," *IEEE Trans. Industrial Informatics*, vol. in press, 2018.
- [9] C. Keerthisinghe, G. Verbič, and A. C. Chapman, "A fast technique for smart home management: Adp with temporal difference learning," *IEEE Transactions on Smart Grid*, vol. 5, pp. 94–104, 2016.
- [10] J. Leadbetter and L. Swan, "Battery storage system for residential electricity peak demand shaving," *Energy and Buildings*, vol. 55, no. 3, pp. 685–692, 2012.
- [11] Z. Ren, G. Grozev, and A. Higgins, "Modelling impact of pv battery systems on energy consumption and bill savings of australian houses under alternative tariff structures," *Renewable Energy*, vol. 89, no. 3, pp. 317–330, 2016.
- [12] D. Lifschitz and G. Weiss, "Optimal energy management for grid-connected storage systems," *Optimal control applications and methods*, vol. 36, no. 4, pp. 447–462, 2014.
- [13] E. Ratnam, S. Weller, and C. Kellett, "An optimization-based approach to scheduling residential battery storage with solar pv: Assessing customer benefit," *Renewable Energy*, vol. 75, no. 4, pp. 123–124, 2017.
- [14] P. Scott, S. Thiebaux, M. van den Briel, and P. Van Hentenryck, "Residential demand response under uncertainty," Australian National University, University of Melbourne, NICTA, Tech. Rep., 2013, [Online]. Available: <http://users.cecs.anu.edu.au/~pscott/extras/papers/scott2013.pdf>. [Accessed: October 2, 2017].
- [15] J. Widen, A. Nilsson, and E. Wackelgard, "A combined markov-chain and bottom up approach to modelling of domestic lighting demand," *Energy and Buildings*, vol. 41, pp. 1001–1012, 2009.
- [16] I. Richardson, M. Thomson, and D. Infield, "A high resolution domestic building occupancy model for energy demand simulations," *Energy and Buildings*, vol. 40, no. 8, pp. 1560–1566, 2008.
- [17] J. Page, D. Robinson, N. Morel, and J. Scartezini, "A generalised stochastic model for the simulation of occupant presence," *Energy and Buildings*, vol. 40, pp. 83–98, 2008.
- [18] I. Richardson, M. Thomson, D. Infield, and A. Delahunty, "Domestic lighting: A high-resolution energy demand model," *Energy and Buildings*, vol. 41, no. 7, pp. 781–789, 2009.
- [19] I. Richardson, M. Thomson, D. Infield, and C. Clifford, "Domestic electricity use: A high resolution energy demand model," *Energy and Buildings*, vol. 42, no. 10, pp. 1878–1887, 2010.
- [20] M. Hofmann, S. Riechelmann, C. Crisosto, R. Mubarak, and G. Seckmeyer, "Improved synthesis of global irradiance with one-minute resolution for pv system simulations," *International Journal of Photoenergy*, vol. 165, pp. 445–461, 2017.

- [21] J. Bright, C. Smith, P. Taylor, and R. Crook, "Stochastic generation of synthetic minutely irradiance time series derived from mean hourly weather observation data," *Solar Energy*, vol. 115, pp. 229–242, 2015.
- [22] E. McKenna and M. Thompson, "High-resolution stochastic integrated thermal-electric domestic demand model," *Applied Energy*, vol. 165, pp. 445–461, 2016.
- [23] D. Dusabe, J. Mundah, and A. Jimoh, "Modelling of cloudless solar radiation for pv module performance analysis," *Journal of Electrical Engineering*, vol. 60, no. 4, pp. 192–197, 2009.
- [24] I. Richardson and Thomson, "Integrated simulation of photovoltaic micro-generation and domestic electricity demand: a one-minute open-source model," *Proceedings of the Institution of Mechanical Engineers*, vol. 227, no. 1, pp. 73–81, 2013.
- [25] J. MacQueen, "Some methods for classification and analysis of multivariate observations," *Proceedings of the Fifth Berkeley Symposium on Mathematical Statistics and Probability*, vol. 1, pp. 281–297, 1967. [Online]. Available: <https://projecteuclid.org/euclid.bsm/1200512992>. [Accessed: Sep 30, 2017].
- [26] Y. Raykov, A. Boukouvalas, F. Baig, and M. Little, "What to do when k-means fails: a simple yet principled alternative algorithm," *PLoS ONE*, 2016, [Online]. Available: <http://journals.plos.org/plosone/article?id=10.1371/journal.pone.0162259>. [Accessed: May 26, 2017].
- [27] "Distributed generation and distributed storage: Sgsc technical compendium," Ausgrid, Tech. Rep., 2014, [Online]. Available: <http://www.ausgrid.com.au/Common/Custom-Service/Homes/Solar-power-and-batteries/Battery-Trials.aspx>. [Accessed: May 30, 2017].
- [28] P. Breheny, "Kernel density estimation," University of Kentucky, Tech. Rep., [Online]. Available: <https://web.as.uky.edu/statistics/users/pbreheny/621/F10/notes/10-28.pdf>. [Accessed: Oct 1, 2017].
- [29] D. Jenkins, S. Patidar, and S. A. Simpson, "Synthesising electrical demand profiles for uk dwellings," *Energy and Buildings*, vol. 76, pp. 605–614, 2014.
- [30] T. Ferguson, "A bayesian analysis of some nonparametric problems," *The Annals of Statistics*, vol. 1, no. 2, pp. 209–230, 1973.
- [31] Y. Teh, "Dirichlet process," University College London, Tech. Rep., 2010, [Online]. Available: <https://www.stats.ox.ac.uk/~teh/research/npbayes/Teh2010a.pdf>. [Accessed: May 25, 2017].
- [32] Y. Teh, D. Gorur, and Z. Ghahramani, "Stick-breaking construction for the indian buffet process," Presented at the Eleventh International Conference on Artificial Intelligence and Statistics, Tech. Rep., 2007, [Online]. Available: <https://www.stats.ox.ac.uk/~teh/papers.html>. [Accessed: May 26, 2017].
- [33] K. Heller, Y. W. Teh, and D. Gorur, *Infinite Hierarchical Hidden Markov Models*, ser. Proceedings of Machine Learning Research, D. van Dyk and M. Welling, Eds. Hilton Clearwater Beach Resort, Clearwater Beach, Florida USA: PMLR, 16–18 Apr 2009, vol. 5. [Online]. Available: <http://proceedings.mlr.press/v5/heller09a.html>
- [34] B. Frigyi, A. Kapila, and M. Gupta, "Introduction to the dirichlet distribution and related processes," University of Washington, Tech. Rep., 2010, [Online]. Available: <https://www2.ee.washington.edu/techsite/papers/refer/UWEETR-2010-0006.html>. [Accessed: May 25, 2017].
- [35] Y. Teh, "A tutorial on dirichlet processes and hierarchical dirichlet processes," Gatsby Computational Neuroscience Unit, University College London, presented at CUED 2007, Tech. Rep., 2007, [Online]. Available: <http://mlg.eng.cam.ac.uk/tutorials/07/ywt.pdf>. [Accessed: May 26, 2017].
- [36] J. Rice, *Mathematical Statistics and Data Analysis*. Brooks Cole Cengage Learning, 2007.
- [37] T. Power and G. Verbič, "A nonparametric bayesian model for forecasting residential solar generation," *2017 Australasian Universities Power Engineering Conference (AUPEC)*, pp. 1–6, 2017.
- [38] "Smart grid, smart city," Australian Government Department of Environment and Energy, Tech. Rep., 2017, [Online]. Available: <http://www.environment.gov.au/energy/programs/smartgridsmartcity>. [Accessed: July 11, 2017].
- [39] R. Hogg, J. McKean, and A. Craig, *Introduction to Mathematical Statistics*. Pearson Education Limited, 2014.